Biomacromolecules

Article

Cite This: Biomacromolecules 2019, 20, 3340−3351

pubs.acs.org/Biomac

Thermoresponsive Protein-Engineered Coiled-Coil Hydrogel for Sustained Small Molecule Release

Lindsay K. Hill,[†,‡,§,∥,⋈] Michael Meleties,[†,⋈] Priya Katyal,[†] Xuan Xie,[†] Erika Delgado-Fukushima,[†] Teeba Jihad,[†] Che-Fu Liu,[†] Sean O'Neill,[⊥] Raymond S. Tu,[⊥] P. Douglas Renfrew,[#] Richard Bonneau,[#,∇,○] Youssef Z. Wadghiri,[§,∥] and Jin Kim Montclare[*,†,∥,◆,¶]

[†]Department of Chemical and Biomolecular Engineering, New York University Tandon School of Engineering, Brooklyn, New York 11201, United States

[‡]Department of Biomedical Engineering, SUNY Downstate Medical Center, Brooklyn, New York 11203, United States

[§]Center for Advanced Imaging Innovation and Research (CAI2R) and [∥]Bernard and Irene Schwartz Center for Biomedical Imaging, Department of Radiology, New York University School of Medicine, New York, New York 10016, United States

[⊥]Chemical Engineering Department, The City College of New York, 160 Convent Avenue, New York, New York 10031, United States

[#]Center for Computational Biology, Flatiron Institute, Simons Foundation, New York, New York 10010, United States

[∇]Center for Genomics and Systems Biology, New York University, New York, New York 10003, United States

[○]Computer Science Department, Courant Institute of Mathematical Sciences, New York University, New York, New York 10009, United States

[◆]Department of Chemistry, New York University, New York, New York 10012, United States

[¶]Department of Biomaterials, New York University College of Dentistry, New York, New York 10010, United States

Supporting Information

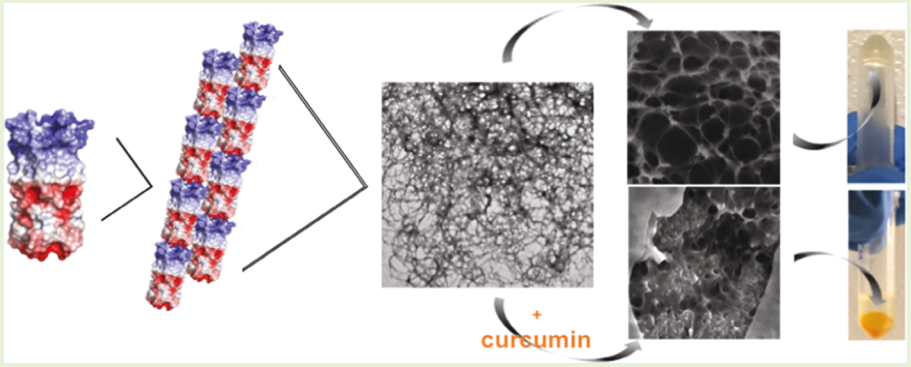

ABSTRACT: Thermoresponsive hydrogels are used for an array of biomedical applications. Lower critical solution temperature-type hydrogels have been observed in nature and extensively studied in comparison to upper critical solution temperature (UCST)-type hydrogels. Of the limited protein-based UCST-type hydrogels reported, none have been composed of a single coiled-coil domain. Here, we describe a biosynthesized homopentameric coiled-coil protein capable of demonstrating a UCST. Microscopy and structural analysis reveal that the hydrogel is stabilized by molecular entanglement of protein nanofibers, creating a porous matrix capable of binding the small hydrophobic molecule, curcumin. Curcumin binding increases the α-helical structure, fiber entanglement, mechanical integrity, and thermostability, resulting in sustained drug release at physiological temperature. This work provides the first example of a thermoresponsive hydrogel comprised of a single coiled-coil protein domain that can be used as a vehicle for sustained release and, by demonstrating UCST-type behavior, shows promise in forging a relationship between coiled-coil protein-phase behavior and that of synthetic polymer systems.

INTRODUCTION

Hydrogels are three-dimensional (3D) crosslinked polymer matrices with a high retention of water that are used in applications including tissue engineering, biomaterial implants, and drug delivery.[1] Although traditional examples of hydrogels have been comprised of synthetic polymers,[2] advances in protein and peptide engineering have resulted in the design of hydrogels possessing specific primary sequences and secondary

Received: January 23, 2019
Revised: July 21, 2019
Published: July 29, 2019

DOI: 10.1021/acs.biomac.9b00107
Biomacromolecules 2019, 20, 3340−3351

structures ideal for drug binding, stimuli responsiveness, cell adhesion, and mechanical integrity.[3] Though substantial work has focused on β-structured systems,[4] α-helical coiled-coil domains composed of two or more α-helices that form a supercoil[5] have also been employed to generate hydrogels. Helical hydrogels include hybrids of the coiled-coil motif and synthetic polymers,[6−8] engineered protein-block co-polymers bearing coiled-coils fused to conformationally distinct domains,[9−18] and coiled-coil peptides.[19−22] These systems have demonstrated evidence of either porous networks[23−29] or interconnected nanofibers, 2.5[19]−20 nm[20] in diameter. Such matrices are physically crosslinked hydrogels, where physical crosslinks are mediated through molecular entanglement or noncovalent interactions including hydrogen bonds, van der Waals, electrostatic, or hydrophobic interactions.[30,31] The physical interactions eliminate the need for potentially toxic chemical crosslinkers and often permit stimuli-responsive behavior.[32] In the case of coiled-coil fusions that form hydrogels, physical crosslinks are formed via reversible intermolecular associations between coiled-coil domains.[32]

Thermoresponsive hydrogels, demonstrating temperature-sensitive solution-to-gel (sol−gel) transitions, are the most widely studied stimuli-responsive gels.[33] Thermoresponsive hydrogels are traditionally described as lower critical solution temperature (LCST)-type hydrogels, which are miscible at lower temperatures and gel when heated above their critical transition temperature (LCST), or upper critical solution temperature (UCST)-type hydrogels that gel when cooled below their critical temperature (UCST).[30] Resilin-based protein-engineered materials are, thus far, the only examples of single-protein-based UCST-type hydrogels; however, these polypeptides require chemical or photochemical crosslinking.[34] Although coiled-coil peptides have been utilized for hydrogel assembly,[19−22] all are comprised of synthetic peptides that do not fit UCST-type hydrogel criteria due to their lack of thermoresponsiveness[19,20] or their dual-peptide composition.[21,22] To date, there are no described thermoresponsive hydrogels, including those with UCST-type behavior, comprised solely of a single coiled-coil protein.

The study described herein investigates the ability of a rationally designed coiled-coil protein, Q,[35,36] to self-assemble into a fibrous network-based hydrogel. This is the first report of a thermoresponsive hydrogel solely comprised of a single α-helical coiled-coil domain. The physically crosslinked Q gel demonstrates a porous network composed of interconnected nanofibers with reversible thermoresponsiveness below and above its UCST, determined to be ∼16.2 °C. The mechanical integrity at 4 °C and thermostability of the hydrogel at 37 °C are both improved upon binding to curcumin (CCM), a model molecule for hydrophobic drugs, permitting a sustained release of the molecule at physiological temperature. This work demonstrates that coiled-coil proteins can independently assemble into a functional physically crosslinked hydrogel with tunable phase behavior.

EXPERIMENTAL SECTION

Materials. M15MA *Escherichia coli* cells were a gift from David Tirrell (California Institute of Technology). Bacto-tryptone, sodium chloride, yeast extract, tryptic soy agar, ampicillin, kanamycin, sodium phosphate monobasic monohydrate ($NaH_2PO_4{\cdot}H_2O$), sodium phosphate dibasic anhydrous (Na_2HPO_4), ammonium chloride (NH_4Cl), potassium phosphate monobasic (KH_2PO_4), sodium hydroxide (NaOH), dextrose monohydrate (D-glucose), magnesium sulfate, calcium chloride ($CaCl_2$), manganese chloride tetrahydrate ($MnCl_2{\cdot}4H_2O$), cobaltous chloride hexahydrate ($CoCl_2{\cdot}6H_2O$), zinc sulfate heptahydrate ($ZnSO_4{\cdot}7H_2O$), boric acid (H_3BO_3), isopropyl β-D-1-thiogalactopyranoside (IPTG), tris−hydrochloride (Tris−HCl), Pierce bicinchoninic acid (BCA) assay kit, Pierce snakeskin dialysis tubing 3.5 kDa molecular weight cut off (MWCO), sodium dodecyl sulfate (SDS), and Molecular Probes FluoSpheres polystyrene microspheres were acquired from Thermo Fisher Scientific. All 20 naturally occurring amino acids, nickel(II) chloride hexahydrate ($NiCl_2{\cdot}6H_2O$), sodium molybdate dihydrate ($Na_2MoO_4{\cdot}2H_2O$), iron(III) chloride ($FeCl_3$), and thiamine hydrochloride (vitamin B), were purchased from Sigma-Aldrich. Copper(II) chloride anhydrous ($CuCl_2$), sodium selenite (Na_2SeO_3), imidazole, and curcumin were purchased from Acros Organics. Hydrochloric acid (HCl) and Coomassie Brilliant Blue G-250 were purchased from VWR. HiTrap immobilized metal affinity chromatography (IMAC) fast flow (FF) 5 mL column for protein purification and Whatman filter paper for transmission electron microscopy (TEM) sample preparation were purchased from GE Healthcare Life Sciences. Macrosep and Microsep Advance centrifugal devices 3 kDa MWCO and 0.2 μm syringe filters were purchased from Pall Corporation. Acrylamide/bis solution (30%) 29:1 and natural polypeptide SDS-polyacrylamide gel electrophoresis (SDS-PAGE) standard were purchased from Bio-Rad. Formvar/carbon-coated copper grids (FCF400-Cu) and 1% uranyl acetate for TEM were purchased from Electron Microscopy Sciences. Silicon wafers for scanning electron microscopy (SEM) were purchased from Ted Pella, Inc.

Protein Expression. Chemically competent M15MA *E. coli* cells,[37] 100 μL in volume, carrying the kanamycin-resistant pREP4 plasmid[38] (Qiagen) were transformed via heat shock with 250 ng of ampicillin-resistant pQE30/Q plasmid[35] maintaining an N-terminal 6× histidine tag (6× His-tag). Transformed cells were allowed to recover in 700 μL lysogeny broth and grown at 37 °C and 300 rpm for 45 min. Transformed cells were then plated onto tryptic soy agar plates containing ampicillin (0.2 mg mL^{-1}) and kanamycin (0.35 mg mL^{-1}) and allowed to grow overnight at 37 °C for approximately 16 h. Ampicillin and kanamycin were used to positively select for M15MA cells containing the plasmid vector. Starter cultures were prepared from single colonies in modified M9 medium (0.5 M Na_2HPO_4, 0.22 M KH_2PO_4, 0.08 M NaCl, and 0.18 M NH_4Cl) containing all 20 natural amino acids (100 μg mL^{-1}), ampicillin (0.2 mg mL^{-1}), kanamycin (0.35 mg mL^{-1}), vitamin B (0.034 mg mL^{-1}), D-glucose (0.1 mg mL^{-1}), magnesium sulfate (0.22 mg mL^{-1}), calcium chloride (0.01 mg mL^{-1}), and trace metals (0.02% (v/v), see the Supporting Information). Starter cultures were incubated at 37 °C and 350 rpm for 16 h. Single starter cultures were added to expression flasks at 4% (v/v) in 400 mL of M9 media, supplemented as described above, and incubated at 37 °C and 350 rpm for approximately 3 h until the optical density at 600 nm was 0.7−0.9. Protein Q expression was induced with IPTG (200 μg mL^{-1}) and returned to 37 °C and 350 rpm for another 3 h. Following protein expression, cells were pelleted by centrifugation at 4 °C and 5000 rpm for 20 min and subsequently stored at −80 °C until purification. Aliquots of 1 mL cell culture were obtained before and 3 h post-IPTG induction for assessment of protein expression via 12% SDS-PAGE bearing a polypeptide ladder. The expression gel was stained with Coomassie Brilliant Blue G-250 and imaged on an ImageQuant 350 imager.

Protein Purification. The Q protein was purified under native conditions at pH 8.0. Cell pellets from 400 mL expressions were thawed and resuspended in 40 mL, 1/10 of the expression volume, of buffer A (50 mM Tris−HCl and 500 mM NaCl, pH 8.0). The cell suspension was placed in an ice water bath and lysed using ultrasonic probe sonication (Q500 sonicator, QSonica) at 45% amplitude, pulse 5 s on and 5 s off, for a total sonication time of 3 min in 1 min intervals. Cellular debris was removed from the crude lysate via centrifugation at 4 °C and 14 000g for 50 min prior to purification via syringe−pump driven immobilized metal affinity chromatography (IMAC) on a cobalt-charged Q sepharose high-performance 5 mL column (HiTrap IMAC FF 5, GE Health Sciences). The protein was eluted using a gradient of buffer B (50 mM Tris−HCl, 500 mM NaCl,

DOI: 10.1021/acs.biomac.9b00107
Biomacromolecules 2019, 20, 3340−3351

500 mM imidazole, pH 8.0) yielding an increase in imidazole concentrations from 10 to 500 mM. All fractions were assessed for purity using 12% SDS-PAGE, stained and imaged as described above. Pure Q protein was typically seen in the elutions containing 100−500 mM imidazole, which were filtered through a 0.2 μm syringe filter and added to snakeskin tubing with a 3.5 kDa MWCO for room-temperature dialysis across six buckets, each containing 5 L of buffer A, to remove imidazole. The Q protein, in both solution and hydrogel state, was maintained in buffer A for all studies.

Hydrogel Preparation and Assessment of Thermoresponsiveness. The protein was concentrated using 3 kDa MWCO Macrosep and Microsep Advance centrifugal devices at 4 °C and 3000 rpm, after which the protein concentration in buffer A was assessed using a BCA assay compared to a standard curve of known albumin concentrations. A sample of the concentrated purified Q protein was diluted to 50 μM, run on 12% SDS-PAGE, and its purity was quantified based on band intensity using the Image Studio Lite software (LI-COR Biosciences). For initial hydrogel formation studies, a 250 μL sample of 2 mM (1.3% w/v) protein Q in buffer A was added to a 2 mL glass vial and placed at 4 °C. Gel formation was visually monitored after 48 h and 96 h. To assess whether the hydrogel was responsive to temperature, it was placed at 37 °C and inverted to determine if the sample remained in the gel state or transitioned to a solution. For comparison, a 250 μL sample of 2 mM (1.3% w/v) protein Q was added to a 2 mL glass vial and placed at room temperature for 96 h and furthermore up to 2 weeks.

Transmittance Assessment. Concentrated Q solutions (2 mM or 1.3% w/v) in buffer A, 200 μL in volume, were added to a type-21 quartz cuvette with a 1 cm pathlength (BuckScience). Its transmittance at 720 nm, the wavelength at which all protein samples showed a distinct peak in the spectrum, was recorded on a UV−vis Cary-50 (Varian Inc.) equipped with a TC125 temperature regulator (Quantum Northwest). Solution-state samples were first analyzed at room temperature. They were then permitted to gel in the cuvette at 4 °C for 96 h prior to transmittance assessment at 4 °C. Cuvettes were incubated at 37 °C for 30 min to initiate the gel−sol transition, and the transmittance was measured at 37 °C. Samples were cycled between 4 and 37 °C until the transmittance recordings revealed a significant decrease in transmittance, indicative of sample aggregation.

Upper Critical Solution Temperature (UCST) Determination. To determine the UCST, 150 μL of Q samples were prepared at 1−3.5 mM (0.6−2.2% w/v) protein concentration in buffer A and incubated in 2 mL tubes at specific temperatures ranging from 4 to 23 °C (room temperature) (Thermomixer R, Eppendorf). Samples remained at the set temperature for up to 2 weeks and were inverted to check for gelation. If gelation was not observed after 2 weeks, the conditions were deemed unsuitable for gel formation, and the sample was considered to be a solution in its equilibrium state. A phase diagram was created by plotting the concentration with respect to temperature for each experimental condition. The gelled samples on the sol−gel boundary were then fitted to a third-order nonlinear regression[39,40] to interpolate points on the phase boundary not feasibly achieved experimentally due to limitations of the heating instrumentation, which was strictly programmable in increments of 1 °C. Specifically, the fit was used to predict the UCST as the maximum point on the solubility curve.[41]

Microrheology. The sol−gel transition was characterized at the microscale using passive microrheology, as described by O'Neill et al.[42] Briefly, Molecular Probes FluoSpheres polystyrene microspheres, 1 μm in diameter, were added to a room-temperature solution of 2 mM (1.3% w/v) Q in buffer A resulting in 4% (v/v) bead content within the protein solution. The bead−protein sample was loaded via pipette onto a microscopy slide fitted with an elevated coverslip to create a channel for the sample addition and subsequent gelation. The slide was imaged at 0 h and subsequently every 12 hours, up to 144 h (6 days), until bead movement was no longer detectable. Between measurements, the sample was left to incubate at 4 °C fastened to a laboratory rotisserie (Labquake Rotisserie, Barnstead Thermolyne) rotating at 8 rpm, allowing for gel formation while preventing bead settling. For each time point, sample slides were imaged on a Leica DMI4000 B automated inverted microscope at 40× magnification using an N21 filter (Leica Microsystems). The Brownian motion of the particles was recorded for 300 frames at 27 frames s^{-1}. The resulting images were stacked and converted to grayscale using New York University High Performance Computing. Video files were used to track the mean squared displacement (MSD), Δr^2, of the beads' Brownian motion as a function of time (τ) in seconds, as described in eq 1, following a protocol developed by Larsen and Furst[43] with MATLAB (MathWorks) algorithms developed by Dufresne, Kilfoil, and Blair[44−46] and modified by O'Neill et al.[42]

$$\mathrm{MSD} = \Delta r^2(\tau) \tag{1}$$

$$\mathrm{d}\ln(\Delta r^2(\tau))/\mathrm{d}\ln\tau = 1 \tag{2}$$

The logarithmic slope of the initial 0 h MSD data of the pre-gelation room-temperature Q protein solution was defined by eq 2, where its logarithmic slope of ∼1 indicates the Brownian diffusion of particles within a viscous liquid or solution-state material.[47] All subsequent MSD curves were mathematically superimposed onto the 0 h curve to determine the time at which the data diverged, indicating the sol−gel transition time or critical gel time (t_c), when the material transitions from a solution state to a gel-state network. Due to the similar shape of the MSD curves throughout the experiment, superimposition of the curves is achievable by empirical shifting of the data into solution-state and gel-state master curves.[47] Superimposition was, therefore, achieved by multiplying post-0 h MSD curves horizontally by the relaxation time shift factor a and vertically by the creep compliance shift factor b in an attempt to overlay them onto the 0 h curve, creating the solution-state master curve, until the time point at which the data could no longer be aligned. This point of divergence is indicative of the sol−gel transition, and remaining curves were instead superimposed onto the final post-gelation curve, forming a gel-state master curve. The solution-state and gel-state master curves intersect at t_c, with the logarithmic slope at this intersection corresponding to the critical relaxation exponent (or viscoelastic exponent), n_c.[47] Therefore, whether the logarithmic slope of the MSD curve at a given time point is greater than or less than n_c determines whether it is in the solution state or gel state, respectively. Furthermore, the value of n_c is indicative of the connectivity within crosslinked systems, where $0.5 < n_c < 1$ is indicative of a loosely crosslinked gel and $0.1 < n_c < 0.5$ indicates a densely crosslinked gel.[47−51] Plotting the shift factors a and b of each curve against time (h) allows for a more precise calculation of t_c. Upon determination of t_c, this value was used to find the dynamic scaling exponents, namely, the relaxation time exponent (y) and the creep compliance exponent (z). The values of y and z are equal to the slope of a logarithmic plot of each curve's shift factors a and b, respectively, against the difference between the time at which that curve was acquired and t_c. The value of n_c was then calculated as z/y. All analyses were performed independently for three protein samples, and the averaged logarithmic slope of MSD, t_c, y, z, and n_c values, along with the corresponding standard deviations, were reported.

Modeling of Q-CCM Binding. CCM conformer libraries were generated using the BioChemical Library ConformerGenerator application.[52] Docking between the Q protein and CCM was performed using Rosetta (RosettaCommons) with the ligand transform protocol.[53] The docking protocol was used to simultaneously sample ligand conformations, while allowing for flexibility in both the side chains and backbone of the protein. Due to the long, narrow axial pore of the Q protein, five independent runs were conducted where the starting position of CCM was adjusted to scale the full length of the cavity. Models (500) were generated from each starting conformation for a total of 2500 models.

Curcumin Binding, Release, and Hydrogel Erosion. The hydrogel was assessed for its ability to bind CCM as was previously demonstrated by Q fibers in solution.[35,36] A 150 μL aliquot of Q protein concentrated to 2 mM (1.3% w/v) was added to a 2 mL Eppendorf tube and placed at 4 °C for 96 h to allow for gel formation. A 300 μL volume of 1 mM CCM solution (in buffer A containing 5% dimethyl sulfoxide (DMSO)) was added atop the gel and returned to

DOI: 10.1021/acs.biomac.9b00107
Biomacromolecules 2019, 20, 3340−3351

4 °C. The sample was incubated at 4 °C for 48 h, permitting absorption of CCM by the gel. As a control, 300 μL of 5% DMSO in buffer A, excluding CCM, was added atop separate gels and identically assessed. Following the absorption period of 48 h, control Q and CCM-bound Q (Q·CCM) gels were gently centrifuged at room temperature and 2500 rpm for 2.5 min, allowing for the collection of the supernatant only. The gels were then washed with fresh 37 °C buffer A to remove nonspecifically bound CCM. The wash buffer was collected and replaced with fresh 37 °C buffer A. The gels were placed at 37 °C and 300 rpm (Thermomixer R, Eppendorf) for the remainder of the gel erosion and drug-release study. At specific time intervals, the gels were again centrifuged at room temperature and 2500 rpm for 2.5 min, 300 μL of the supernatant was collected and replaced with 300 μL of fresh 37 °C buffer, and the samples were returned to 37 °C and 300 rpm between collections. This process was repeated for each time point until the gels had broken down entirely and were unable to pellet upon centrifugation. The collected supernatant samples were subjected to BCA assays to determine the extent of gel erosion. The percent of total protein released from the gel at each time point was plotted.

Simultaneously, collected supernatant samples from Q·CCM were characterized spectrophotometrically for CCM concentration via absorbance at 410 nm. Sample absorption values were compared to a standard curve of known CCM concentrations in buffer A + 5% DMSO that were also incubated at 37 °C and 300 rpm and measured spectrophotometrically throughout the time course. The gel's encapsulation efficiency, calculated by eq 3,[54] and the percent of encapsulated CCM released were plotted.

$$\text{Encapsulation Efficiency} = \frac{\text{mass of CCM added} - \text{mass of unbound CCM}}{\text{mass of CCM added}} \quad (3)$$

Analysis of Curcumin Release Kinetics. To assess the CCM release mechanism from the Q·CCM hydrogel, CCM release data were fitted to zero-order[55] (eq 4), first-order[56] (eq 5), Higuchi[57] (eq 6), and Hixson–Crowell[58] (eq 7) kinetic models. Data were also fitted to the Korsmeyer–Peppas model[59] (eq 8) and a modified Gallagher–Corrigan (G–C) model[60] (eq 9) to assess the contribution of diffusion and erosion on drug release.[59] To obtain the kinetic rate constants and burst parameter, the modified G–C model was fitted to the data using nonlinear regression analysis in MATLAB.[61] In Fickian diffusion, i.e., zero-order kinetics, the drug diffuses from the matrix independent of its concentration.[55] By contrast, for non-Fickian diffusion, several factors can affect drug release, including drug concentration and the surface area or diameter of the drug-release system.[62] In vitro CCM release data were fitted to the kinetic models, and the goodness of fit was determined.

$$Q_t = Q_0 + k_0 t \quad (4)$$

$$\log(Q_t) = \log(Q_0) - k_1 t/2.303 \quad (5)$$

$$Q_t = k_H t^{1/2} \quad (6)$$

$$Q_t^{1/3} = Q_0^{1/3} - k_{HC} t \quad (7)$$

$$\log(M_t/M_\infty) = \log(k_{KP}) + n_{KP} \log(t) \quad (8)$$

$$Q_t = A + X_1(1 - e^{-K_1 t}) + X_2 \frac{e^{-K_2(t_{max}-t)}}{1 + e^{-K_2(t_{max}-t)}} \quad (9)$$

where Q_t is the amount of CCM released at time t, Q_0 is the initial amount of CCM released, k_0 is the zero-order release constant, k_1 is the first-order release constant, k_H is the Higuchi dissolution constant, and k_{HC} is the Hixson–Crowell rate constant. For the Korsmeyer–Peppas model, M_t/M_∞ is the fraction of CCM released at time t, k_{KP} is the release rate constant, and n_{KP} is the release exponent. For the modified Gallagher–Corrigan model, A is the burst parameter; K_1 and X_1 are the kinetic release constant and fraction of CCM released during the burst/diffusion (first) phase of the model, respectively; K_2 and X_2 are the kinetic release constant and fraction of CCM released during the erosion (second) phase of the model, respectively; and t_{max} is the time to reach the maximum release rate.

Rheology. To assess the impact of CCM binding on the gel's mechanical integrity, the rheological properties of the Q and Q·CCM hydrogels were assessed on a stress-controlled rheometer (ARES-G2, TA Instruments) equipped with parallel plate geometry with a lower plate 25 mm in diameter and an upper plate 8 mm in diameter set to 4 °C with a 0.2 mm geometry gap. The Q gel was formed at 2 mM (1.3% w/v) in buffer A at 4 °C, as described above, and assessed via rheology following 6 days at 4 °C, in line with the final day of gelation assessed via microrheology. The Q·CCM gel was also assessed on day 6, after 4 days (96 h) of gelation and 48 h of CCM binding. Excess CCM was washed away with buffer A prior to rheological analysis. The gels were gently transferred from 2 mL tubes onto the 4 °C rheometer plate with the effective sample area matched that of the 8 mm plate. Strain sweep experiments were carried out on the Q gel from 0.1 to 1000% strain to determine the linear viscoelastic region of Q, at which the frequency sweeps for both gels were performed. The gels' storage moduli (G') and loss moduli (G'') were determined as a function of frequency from 0.1 to 10.0 Hz with an oscillation strain of 5%. Triplicate studies of both gels' G' and G'' values were plotted as a function of frequency.

Attenuated Total Reflectance-Fourier Transform Infrared Spectroscopy (ATR-FTIR). ATR-FTIR spectroscopy was performed to assess the secondary structure of Q before and after gelation and CCM binding using a Nicolet 6700 Fourier Transform Infrared Spectrometer equipped with a diamond ATR accessory and a mercury cadmium telluride-A detector. Protein samples, at 2 mM (1.3% w/v), were prepared as described above, where the pregelation solution-state Q samples were maintained at room temperature for 96 h, the Q hydrogel samples were incubated at 4 °C for 96 h, and the CCM-bound Q·CCM hydrogels were prepared by binding the Q hydrogel to CCM for an additional 48 h at 4 °C. First, a background spectrum was obtained by spotting a 5 μL sample of the appropriate buffer onto the diamond surface; its spectrum was acquired at room temperature from 400 to 4000 cm^{-1} with 0.5 cm^{-1} resolution and automatically subtracted from the protein sample spectra subsequently collected, thus eliminating the contribution of water and buffer salts on the protein spectra. A 5 μL sample of 2 mM (1.3% w/v) protein solution or protein hydrogel in buffer A was then spotted onto the diamond surface, and a 128 scan spectrum was acquired at room temperature from 400 to 4000 cm^{-1} with 0.5 cm^{-1} resolution. Spectra for CCM alone, in the absence of Q, were also collected for comparison. The data was analyzed using PeakFit (Systat Software, Inc.), and peak deconvolution with Gaussian function was performed within the amide I region of 1600–1700 cm^{-1}, as previously described.[35,63] Briefly, a second derivative zero baseline correction was performed on the buffer-subtracted sample spectrum.[35,63] The second derivative of each spectrum was investigated to determine the number and relative locations of peaks. Peak deconvolution was then carried out on the original spectrum, keeping the full width at half-maximum of peaks at less than 30 cm^{-1}, and was deemed complete when the coefficient of determination for the overall spectra was $r^2 = 0.99$.[63] Areas under the peaks were calculated by PeakFit for each secondary structure, and their intensities were compared pre- and post-gel formation and post-CCM binding. Secondary structure percentages were reported as the average of three independently prepared samples.

Circular Dichroism (CD) Spectroscopy. The secondary structures of pre-gelation and post-gelation Q were further assessed using CD spectroscopy. CD spectra were collected in triplicate for both samples using a Jasco J-815 CD spectrometer with a PTC-423S single position Peltier temperature control system. Pre-gelation solution-state Q and Q hydrogel samples were prepared at 2 mM (1.3% w/v) as described above for ATR-FTIR spectroscopy via incubation at room temperature or 4 °C, respectively, for 96 h. Additionally, for CD spectroscopy, solution-state and hydrogel Q samples were diluted 200-fold in deionized water (diH_2O) from 2 mM (1.3% w/v) Q to a final concentration of 10 μM and added to

DOI: 10.1021/acs.biomac.9b00107
Biomacromolecules 2019, 20, 3340–3351

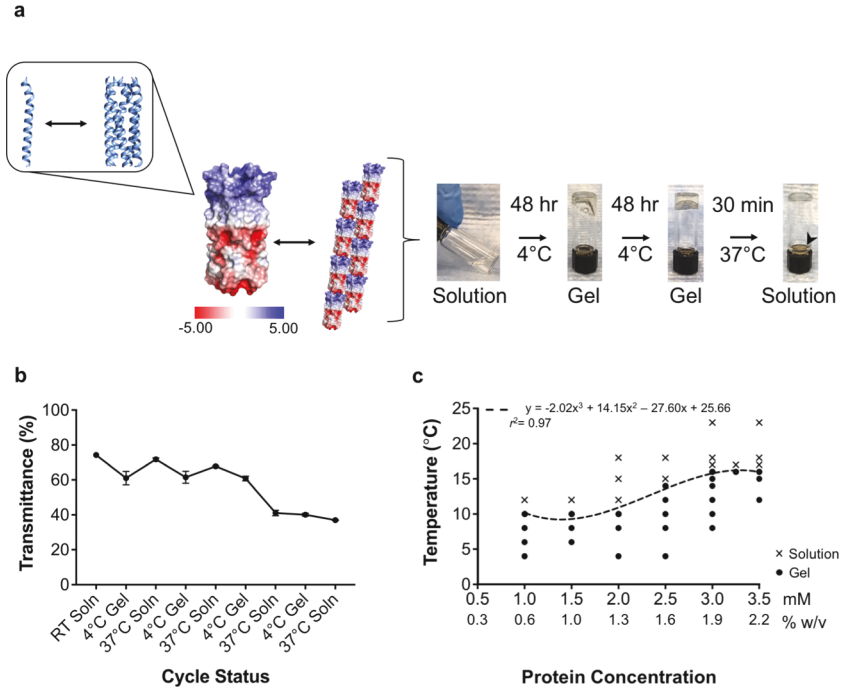

Figure 1. Hydrogel assembly and thermoresponsive phase behavior. (a) Schematic representation of the proposed hierarchical assembly of the Q protein hydrogel from monomeric α-helices to coiled-coil nanofibers at pH 8.0 that interact to form a 3D hydrogel network at 4 °C and transition back to the solution state (arrowhead) at 37 °C. (b) Transmittance of 2 mM (1.3% w/v) Q protein throughout temperature-based cycling between solution and gel states, where each data point represents the average of three independent trials and error bars indicate the standard deviation. (c) Solution-gel phase diagram of Q fitted with a third-order polynomial (dashed line) at the sol−gel boundary to predict the upper critical solution temperature.

quartz cuvettes, yielding the pre-gelation and post-gelation samples, respectively. This dilution was necessary to lower the protein and NaCl content to concentrations suitable for CD measurements. Wavelength spectra were measured at 4 °C from 190 to 250 nm with a step size of 1 nm, a pathlength of 1 mm, and a continuous scanning mode of 20 nm min^{-1}.[36,64−67] Using Jasco spectral analysis software, all Q spectra underwent a buffer spectrum subtraction, using buffer A diluted 200-fold in diH_2O, prior to spectral smoothing via the Savitzky−Golay method set at a convolution width of 13.[68] The mean residue ellipticity (MRE, θ) was calculated from ellipticity values (θ) via eq 10[69]

$$\text{MRE},\quad \theta = \frac{\theta}{10 \times \text{protein conc.} \times \text{path length} \times \text{residue number}} \tag{10}$$

The difference in α-helical content between pre- and post-gelation Q was evaluated by comparing the ratios of the MRE at 208 and 222 nm ($\theta_{222}/\theta_{208}$), where a ratio of 0.8−0.9 typically describes isolated α-helices.[70] The data represent the average of three independently prepared samples.

Transmission Electron Microscopy (TEM). TEM was employed to visualize the assembly of Q on the nanoscale pre- and post-gelation and post-CCM binding. Both solution-state and gel-state Q samples were diluted in buffer A to 50 μM protein concentration at room temperature immediately before TEM spotting. Samples were spotted at room temperature onto Formvar/carbon-coated copper grids at 3 μL volume for 1 min. The samples were blotted with a filter paper, washed with 5 μL diH_2O, and again blotted with the filter paper. The grids were subsequently treated with 3 μL of 1% uranyl acetate for 1 min to negatively stain the spotted protein and blotted dry. All TEM images were acquired at an accelerating voltage of 120 kV on a JEOL JEM-1400 LaB6 soft bio transmission microscope. The diameters of imaged protein assemblies were measured using the ImageJ software.[71]

Scanning Electron Microscopy (SEM). Topographical information of the Q gel in the presence and absence of CCM was acquired on a MERLIN field emission scanning electron microscope (Carl Zeiss AG). For comparison, room-temperature Q solution was also assessed. The pre-gelation solution-state Q samples were prepared by spotting 5 μL of 2 mM (1.3% w/v) room-temperature Q in buffer A solution onto a silica wafer, which was dried in a vacuum desiccator for 3 h. For post-gelation samples, a 5 μL aliquot was taken from the 2 mM (1.3% w/v) Q gel formed in buffer A at 4 °C, in the presence or absence of CCM, and spotted onto the wafer prior to drying for 3 h. All samples were iridium-coated to 3 nm using a high-resolution sputter coater 208HR (Cressington Scientific Instruments) prior to image acquisition for improved contrast.

Statistical Analysis. GraphPad Prism (GraphPad Software) was employed for statistical analysis using student's *t*-test.

RESULTS AND DISCUSSION

Rationale. Although coiled-coil domains have proven to be successful hydrogel components[6−17,19−22] for designing networked systems, they have either been paired with a second coiled-coil motif for heterodimeric assemblies[21,22] or fused to other distinct motifs.[6−18,72] This work explores the creation of a single α-helical coiled-coil self-assembling domain system for the production of thermoresponsive hydrogels. Based on the coiled-coil domain of the cartilage oligomeric matrix protein (COMPcc), Q has been designed and has previously exhibited robust nanofiber and CCM-dependent mesofiber assembly under acidic conditions.[35,36,73] Surface charge distribution, predicted by Adaptive Poisson−Boltzmann solver (APBS)[74] and visualized using PyMOL (Schrödinger, LLC),[75] demonstrates that the charged surface patches previously described of Q under acidic conditions[35] are significantly retained at pH 8.0 (Figure 1a). Therefore, the hierarchical self-assembly of Q into nanofibers through intermolecular associations between coiled-coil pentamers,[35]

DOI: 10.1021/acs.biomac.9b00107
Biomacromolecules 2019, 20, 3340−3351

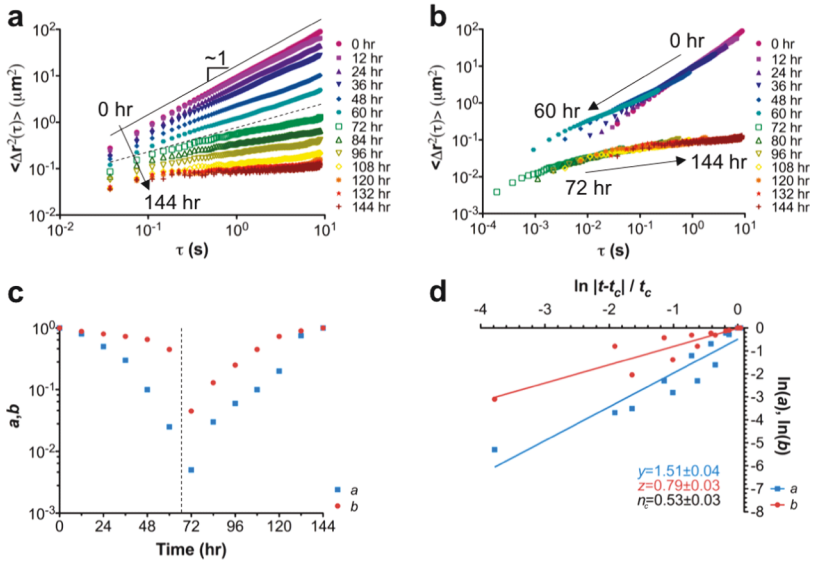

Figure 2. Microrheological determination of sol−gel transition time. (a) Representative particle mean squared displacement (MSD) as a function of time for Q maintained at 4 °C presented as a log−log plot. (b) Superposition of the MSD data in the panel (a) where data from 12 to 144 h was shifted horizontally by factor *a* and vertically by factor *b* to reveal changes in Q's viscoelastic properties over 144 h. (c) Shift factors for time (*a*, blue) and MSD (*b*, red) required for the superposition shown in panel (b) where the critical gel time t_c is determined as the time at which a large shift in *a* or *b* is seen (dashed line). (d) Relaxation time (*a*, blue) and MSD (*b*, red) plotted against the distance from t_c to determine the critical scaling exponents *y* and *z* and the critical relaxation exponent n_c. The values of *y*, *z*, and n_c represent the average values and standard deviations among three independent studies of Q.

and subsequent hydrogel formation, is investigated here. Notably, Q is able to undergo sol−gel transition in a temperature-dependent manner, exhibiting UCST-type hydrogel behavior.

Hydrogel Formation and Thermoresponsiveness. To determine the appropriate conditions for hydrogel formation, biosynthesized (Figure S1) and purified (Figure S2) Q protein was concentrated to 2 mM (1.3% w/v) in buffer A (50 mM Tris−HCl, 500 mM NaCl, pH 8.0) prior to incubation at room temperature or 4 °C. Q left at room temperature showed no gelation within a 2 week time frame. However, Q incubated at 4 °C assembled into a soft hydrogel within 48 h and a firm gel, capable of being physically inverted, within 96 h (Figure 1a). Upon subsequent incubation at 37 °C, typical UCST-type thermoresponsive behavior was observed where the gel transitioned back to the solution state in 30 min (Figure 1a), in agreement with the well-characterized reversibility between coiled-coil interactions via alterations in temperature, pH, and/or salt concentration.[9,30,32,76−78]

To assess the reversibility of the temperature-dependent gelation of Q, the transmittance of Q was monitored via UV−vis spectroscopy while cycling between the solution state at 37 °C and the gel state at 4 °C (Figure 1b). The initial transmittance of concentrated pre-gelation solution-state Q at room temperature was 74.3 ± 0.3%, which decreased to 61.0 ± 3.9% following gelation at 4 °C for 96 h. After gel−sol transition at 37 °C for 30 min, the transmittance increased to 71.7 ± 0.8%. The protein continued to regel and solubilize within 96 h and 30 min, respectively, resulting in similar gel-state and solution-state transmittance values for two subsequent gelation cycles and confirming that the thermoresponsiveness of Q was reversible. However, after the third 37 °C incubation, aggregation was observed, and the transmittance decreased to 41.1 ± 1.5%. Surprisingly, the sample again regelled at 4 °C within 96 h even with apparent aggregation and a transmittance ≤40.1%.

A phase diagram was generated from Q samples incubated from 4 to 23 °C (room temperature) at 1−3.5 mM (0.6−2.2% w/v) protein concentration (Figure 1c). As expected, more concentrated samples gelled at higher temperatures, resulting in a system whose phase behavior could be manipulated by altering the protein concentration.[41] The temperature for gelation plateaued at 16 °C for the highest studied protein concentrations of 3−3.5 mM (1.9−2.2% w/v). A third-order polynomial was then fitted to the gelled samples at the sol−gel boundary[39,40] to predict the UCST, the maximum point on the sol−gel curve below which the system would be in the gel state and above which it would remain in solution.[41] The maximum point on the fitted curve provided a UCST prediction of 16.2 °C at a concentration of 3.3 mM (2.1% w/v) (Figure 1c, dashed line). This work confirmed that the Q hydrogel demonstrated UCST-type behavior with a UCST that was determined experimentally and closely predicted by curve fitting.

Sol−Gel Transition. To quantify the sol−gel transition time t_c of the hydrogel at 4 °C, passive microrheology was employed, and the Brownian motion of fluorescent beads was tracked by their MSD within Q from the solution to hydrogel state as demonstrated via representative microrheological analyses of Q (Figures 2 and S3). This temperature was investigated here and in subsequent gelation studies given the reproducible access to 4 °C conditions. Over 6 days (144 h), the logarithmic slope of the particle MSD decreased from 0.99 ± 0.04 $\mu m^2\ s^{-1}$, consistent with a viscous solution, to 0.17 ± 0.03 $\mu m^2\ s^{-1}$, suggesting that the viscous solution became viscoelastic[47] (Figures 2a, S3, and Table S1). MSD curves were superimposed to identify the time at which there was a divergence in the data, indicative of the sol−gel transition.[42] Q demonstrated a divergence between the 60 and 72 h curves (Figures 2b and S3), illustrating a sol−gel transition time between these timepoints. By plotting the shift factors *a* and *b* against time, t_c was calculated to be 70.4 ± 0.1 h (Figures 2c

DOI: 10.1021/acs.biomac.9b00107
Biomacromolecules 2019, 20, 3340−3351

and S3). The determination of t_c was used to calculate the dynamic scaling exponents y and z from which the critical relaxation exponent n_c, defined as z/y, was determined to be 0.53 ± 0.03 (Figures 2d and S3). Logarithmic slopes greater than n_c, at 0−60 h timepoints, corresponded to a viscoelastic liquid or solution state and logarithmic slopes lower than n_c, at 72−144 h timepoints, were indicative of the viscoelastic solid state (Figures 2a, S3, and Table S1). Based on this n_c value, the Q hydrogel was at the boundary ($n_c \sim 0.5$) of a loosely crosslinked, or porous, gel and a gel densely crosslinked through the entanglement of linear polymers by strong hydrodynamic interactions.[47]

Effects of Curcumin Binding on Hydrogel Erosion and Release. Given previous reports of CCM binding by Q fibers in solution,[35,36] this study sought to test the ability of the Q hydrogel to encapsulate the yellow-colored polyphenolic molecule CCM. First, protein modeling of Q revealed that the protein's long, internal hydrophobic pore varies in diameter, with the widest part being a pentalobular void formed near the N-terminus due to a kink induced by alanine and proline in the 65th and 66th residue positions, respectively (Figure 3). Of the

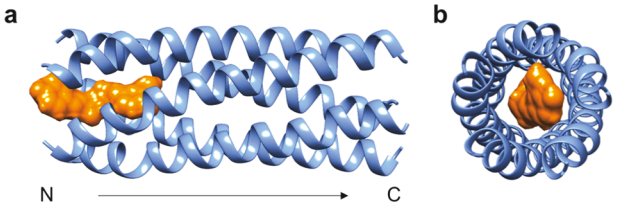

Figure 3. Modeling of Q·CCM Binding. The lowest-energy model from docking simulations illustrating CCM binding by the Q protein at its N-terminal pentalobular void, the widest part of the protein's hydrophobic pore in the (a) axial view and (b) cross-sectional view of the N-terminus.

2500 possible models, the lowest-energy model predicted that this N-terminal hydrophobic cavity would be capable of accommodating the majority of the CCM molecule, with a total energy of −785.2 Rosetta Energy Units. Motivated by the docking prediction, the Q hydrogel was incubated with equimolar CCM at 4 °C. After 48 h, the entire hydrogel was yellow (Figure S4), suggesting uniform distribution of CCM throughout the Q·CCM gel. Control Q gels, incubated in the absence of CCM did not exhibit any color, as expected. From the amount of CCM remaining in the solution and that removed during wash steps, the encapsulation efficiency of CCM within the Q·CCM hydrogel was calculated to be 52.3 ± 0.9%.

Erosion of the hydrogel in the presence and absence of CCM was tracked until the gel completely degraded at 37 °C. The control Q gel demonstrated rapid erosion (Figure 4a, open black diamond), with complete solubilization by 2 h. By contrast, Q·CCM gels (Figure 4a, open orange diamonds) revealed that 19.4 ± 1.5% of the protein hydrogel was solubilized at 2 h and 58.4 ± 4.0% solubilized at 6 h. After 24 h, the Q·CCM gel erosion slowed to 1.6 ± 1.6% encapsulated protein per day through 288 h (day 12), at which point there was again increased erosion to 2.3 ± 1.3% per day, until complete gel degradation was observed at 408 h (day 17) or 432 h (day 18), or 17.7 ± 0.6 days on average, 212-fold slower than the unbound Q hydrogel. The rapid erosion of the control Q gel at 37 °C reflected typical UCST-type hydrogel behavior,[30,77] with a gel−sol transition above its UCST.

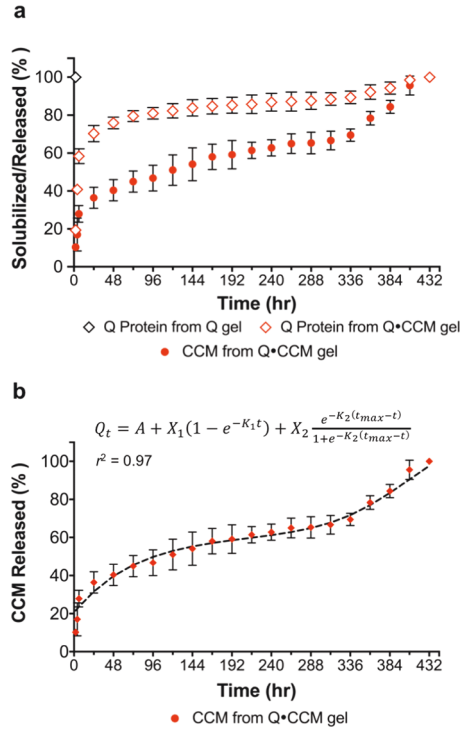

Figure 4. Hydrogel erosion and curcumin release at physiological temperature. (a) Cumulative percent Q protein solubilized from the control Q gel and the curcumin-bound Q·CCM gel, as well as the cumulative percent of curcumin released from the Q·CCM gel, at 37 °C. (b) Cumulative CCM released from the Q·CCM gel fitted to the modified Gallagher−Corrigan model of drug release. All points represent the average of three trials, and error bars indicate the standard deviation.

However, the Q·CCM gel eroded at a significantly slower rate, suggesting that CCM binding possessed a stabilizing effect on the assembled hydrogel, slowing its rate of solubilization or erosion and increasing its potential for sustained drug release.

Tracking of CCM release from the Q·CCM gel was conducted in tandem with erosion studies (Figure 4a, filled orange circles). The Q·CCM gels released 10.3 ± 0.7% of the encapsulated CCM to the supernatant at 2 h and cumulative 27.9 ± 4.4% at 6 h. CCM release slowed to 2.9 ± 2.3% per day from 24 h (day 1) to 288 h (day 12), at which point there was an increased release rate of 6.7 ± 3.4% per day, until the Q·CCM gels were completely eroded, and all CCM had been released to the surrounding buffer at 17.7 ± 0.6 days.

Of the models used in assessing CCM release from the Q·CCM gel, the modified G−C model demonstrated the best fit (r^2 = 0.97) (Figures 4b, S5, and Table 1). Fitting to the model

Table 1. CCM Release Model Parameters Evaluated Using the Modified Gallagher−Corrigan Model

A (%)	X_1 (%)	K_1 (h^{-1})	X_2 (%)	K_2 (h^{-1})	t_{max} (h)	r^2
21.6	40.3	0.013	59.7	0.020	408	0.97

suggested that drug release initially occurred via a burst effect followed by a sustained release, with matrix degradation dominating CCM release in the latter stage[60] (Figure 4b). Comparison of the rate constants, in which $K_2 > K_1$ (Table 1), indicates that the release of CCM due to matrix erosion occurred at a faster rate than the release of CCM through

DOI: 10.1021/acs.biomac.9b00107
Biomacromolecules 2019, 20, 3340−3351

diffusion.[61] The described predictions for the CCM release were in agreement with visual inspections of Q·CCM gels throughout the study (Figure S4). The Q·CCM hydrogel, therefore, showed potential as a vehicle for sustained drug release over 17−18 days.

Mechanical Integrity. Macroscopic mechanical properties of the hydrogel pre- and post-CCM binding were assessed via rheological analysis of the storage and loss moduli (G' and G'', respectively). Strain sweep assessment of the Q hydrogel pre-CCM binding revealed a linear viscoelastic region at 0.3−19.9% strain (Figure S6). A strain of 5% was, therefore, used for all subsequent frequency sweeps of Q hydrogels both pre- and post-CCM binding. At 4 °C, both sets of Q samples were elastic in nature with G' values exceeding their respective G'' values, indicating a gel state (Figures 5, S7, and Table S2). The addition of CCM increased hydrogel elasticity as demonstrated by an increased final G', at 10.0 Hz, from 50.4 Pa for the Q gel to 88.0 Pa for the Q·CCM gel (Table S2). For hydrogels, a higher G' is directly related to increased physical crosslinking or entanglement,[79] suggesting that Q·CCM's higher G' compared to that of the nonbound Q gel indicates an increased degree of crosslinking or entanglement within the sample. These findings are in agreement with the previous work on a COMPcc domain-containing protein-block copolymer hydrogel that demonstrated increased G' following CCM binding, suggesting that CCM indeed improved the protein network and hydrogel assembly.[13]

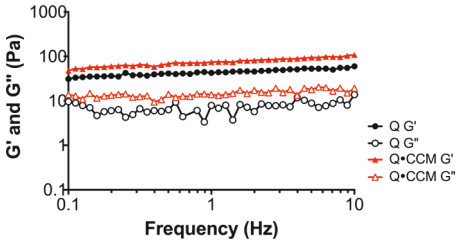

Figure 5. Rheological properties of the Q hydrogel in the presence and absence of curcumin. Representative rheological assessment of the storage (G') and loss (G'') moduli of Q and Q·CCM hydrogels at 4 °C under 5% oscillatory strain.

Secondary Structural Changes upon Gelation and Curcumin Binding. ATR-FTIR spectroscopy was performed to assess the secondary structure of Q from the solution state to the gel state and following CCM binding. Peak deconvolution of the amide I region allowed for quantification of the protein's secondary structure, including its α-helicity[80] (Figures S8, S9, and Table S3). Measurements of the pre-gelation solution-state Q revealed 46% α-helicity (Figures S8a, S9a,b, and Table S3), which increased to 52% in the Q hydrogel (Figure S8b, S9c,d, and Table S3). This increase in α-helicity upon gelation was also confirmed by circular dichroism (CD) measurements (Figure S10 and Table S4). CD spectra of Q both pre- and post-gelation displayed the characteristic α-helical signature (Figure S10). A comparison of the MRE ratios at 208 and 222 nm ($\theta_{222}/\theta_{208}$)[81] revealed an increase in the α-helical character from the pre-gelation state to the post-gelation state with 0.70 and 0.85, respectively (Table S4). Increased α-helicity upon gelation may result from the physical crosslinking between coiled-coil domains via intra- and intermolecular interactions, including hydrophobic and electrostatic interactions as well as hydrogen bonding.[20,82] Following CCM binding, α-helicity assessed via ATR-FTIR spectroscopy increased to 69%, for an overall 23% increase in α-helicity from the pre-gelation state (Figures S8c, S9e,f, and Table S3). Notably, CCM alone does not contribute to the amide I signal on ATR-FTIR spectroscopy (Figure S9g,h). Therefore, the α-helical coiled-coil content increased as Q assembled into a hydrogel and was further stabilized by CCM binding, consistent with previous studies of Q fibers under acidic conditions that also demonstrated increased α-helicity by ATR-FTIR spectroscopy following CCM binding.[35] Hydrophobic interactions between the small molecule and the hydrophobic *a* and *d* residues within Q's axial pore may further

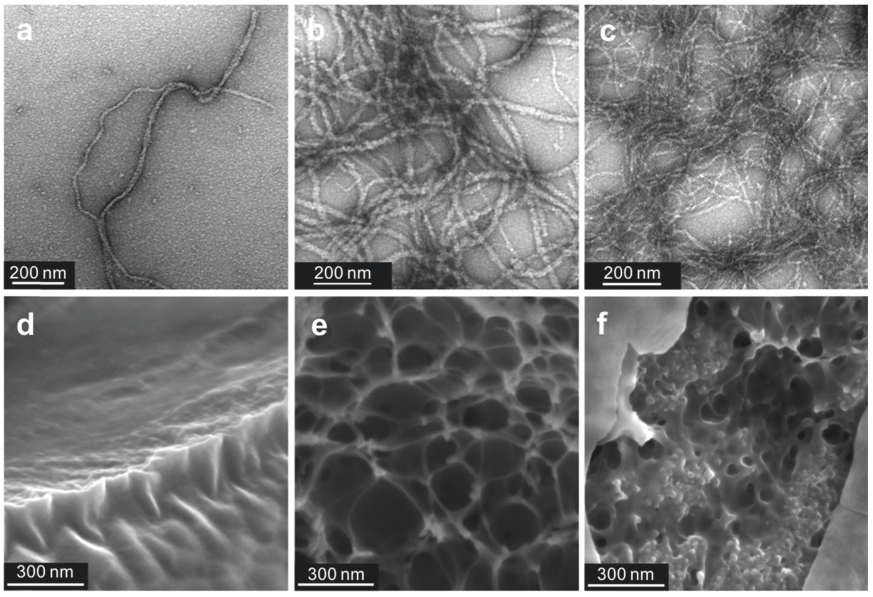

Figure 6. Nanofiber assembly and network formation by Q protein. Transmission electron micrographs of the (a) pre-gelation solution-state Q protein; (b) the Q hydrogel prior to CCM binding; and (c) the CCM-bound Q·CCM gel. Scanning electron micrographs of the (d) pre-gelation solution-state Q protein; (e) the Q hydrogel prior to CCM binding; and (f) the Q·CCM gel.

DOI: 10.1021/acs.biomac.9b00107
Biomacromolecules 2019, 20, 3340−3351

stabilize the coiled-coil assembly, explaining the increase in α-helicity revealed by ATR-FTIR following CCM binding.

Nanoscale Assembly. To determine whether the Q hydrogels were comprised of coiled-coil assembled fibers, transmission electron microscopy (TEM) was performed (Figure 6a−c). As expected, pre-gelation solution-state Q revealed nanofiber assembly averaging 17.5 ± 3.3 nm (N = 50) in diameter and microns in length (Figure 6a). This size was similar to the 10−15 nm diameters previously observed in the parent protein at pH 8.0[81] but smaller than the 20−560 nm diameter Q fibers described at pH 4.0.[35] Although APBS predictions of the Q protein at pH 8.0 revealed that positively and negatively charged surface patches were maintained, ionic shielding due to the presence of 500 mM NaCl within the buffer may weaken the electrostatic interactions between pentamers. In previous studies, at pH 4.0 with 0 mM NaCl, strongly charged surface patches on the Q protein formed robust electrostatic interactions to yield 20−500 nm diameter nanofibers that did not allow for gelation.[35,36] Here, by allowing Q to assemble at pH 8.0 in the presence of 500 mM NaCl, the electrostatic interactions are likely reduced, allowing for fiber assembly to occur predominantly via head-to-tail arrangements of the coiled-coils[20] with reduced lateral assembly, as previously described for the parent COMPcc^S protein.[81] Solution-state Q demonstrated isolated fibers with minimal interconnections (Figure 6a). By contrast, fibers observed in the gels were highly interconnected creating a mesh network (Figures 6b,c and S11) similar to those in reported coiled-coil containing hydrogels,[19,20] indicating that the Q hydrogel was formed through physical crosslinks between coiled-coil fibers.[19,20] Individual fibers within the hydrogel maintained diameters averaging 16.8 ± 3.4 nm (N = 260) (Figure 6b). Imaging of the densest regions of the sample revealed a tight, porous mesh containing fiber bundles 43.8 ± 7.1 nm in diameter (N = 100) (Figure S11a,b), greater than 2-fold the diameters observed in the solution state Q. The Q·CCM gel also demonstrated interconnected fibers averaging 14.5 ± 2.1 nm in diameter (N = 150) (Figure 6c) with fiber bundles averaging 43.4 ± 8.2 nm in diameter (N = 100) (Figure S11c,d). Notably, the Q·CCM gel exhibited tighter nanofiber entanglement and, therefore, a denser meshwork than that of the unbound Q gel (Figures S7 and S11), which may be due to CCM binding not only within Q's hydrophobic pore but also between coiled-coils and coiled-coil nanofibers to be sequestered away from the aqueous buffer environment. This theory is supported by observations in previous fluorescence distribution studies of CCM-bound Q, which suggested that CCM was bound at the pentameric surface as well as the coiled-coil pore.[35]

Hydrogel Microstructure. Hydrogel network topography, both in the presence and absence of CCM, in addition to pre-gelation solution state Q, was analyzed using scanning electron microscopy (SEM). Although solution-state Q demonstrated a nonporous wrinkled pattern (Figure 6d), Q (Figure 6e) and Q·CCM (Figure 6f) gels revealed a porous microstructure similar to that of previously described coiled-coil containing matrices.[16,17,21,24,25] Pore sizes in the unbound Q gel maintained an average diameter of 123.7 ± 26.6 nm (N = 30) (Figure 6e). In the Q·CCM gel (Figure 6f), however, the pore sizes decreased significantly, (****, p < 0.0001) according to an unpaired two-tailed student's t-test, creating a tighter gel network with diameters of 82.4 ± 24.3 nm (N = 20). Together, TEM and SEM results indicated that the improved thermostability (Figure 4a) and mechanical integrity (Figure 5) of the gel following CCM binding resulted from increased nanofiber interactions and subsequent tightening of the porous network.

CONCLUSIONS

Using a rationally designed Q pentameric assembly, we have successfully engineered a thermoresponsive hydrogel composed solely of a single coiled-coil protein domain. Gelation studies demonstrate a reversible thermoresponsive behavior and a concentration-dependent maximum gelation temperature, leading to a UCST phase diagram akin to that of a synthetic polymer solution.[83] Fitting of the phase diagram reveals a UCST point of 16.2 °C and 3.3 mM (2.1% w/v) protein concentration. The hydrogel assembly is driven by physical crosslinks between entangled coiled-coil nanofibers, creating a porous gel ideal for small-molecule encapsulation. In particular, CCM binding by the Q gel results in increased thermostability, mechanical integrity, and α-helicity as well as a tighter network at the nanoscale. Although Q demonstrates traditional UCST-type behavior, via gel−sol transition above the UCST, the CCM-bound gel solubilizes and releases CCM at 37 °C over 17−18 days, within the range of sustained drug-release vehicles.[84] This work opens up the possibility of drawing parallels between the thermoresponsive behavior of protein-based hydrogels and that of synthetic polymer systems, of which a vast array of sol−gel phase diagrams has previously been generated. Future work is already underway to apply the polymer solution theory to the determined phase behavior of Q to rationally design Q variants of different chain lengths to achieve specific UCSTs for tailored thermoresponsive drug release. Furthermore, the effect of pH and ionic strength is being studied to delineate the mechanism of fiber assembly and gel formation.

ASSOCIATED CONTENT

Supporting Information

The Supporting Information is available free of charge on the ACS Publications website at DOI: 10.1021/acs.biomac.9b00107.

Trace metal preparation, TEM, SDS-PAGE of protein expression and purification, microrheology, curcumin-bound hydrogel visualizations, curcumin release kinetics, rheology, ATR-FTIR, and CD (PDF)

AUTHOR INFORMATION

Corresponding Author

*E-mail: Montclare@nyu.edu.

ORCID

Lindsay K. Hill: 0000-0002-1833-8574
Raymond S. Tu: 0000-0002-6192-7665
Jin Kim Montclare: 0000-0001-6857-3591

Author Contributions

⋈L.K.H. and M.M. contributed equally to this work.

Funding

This work was supported by NSF-DMREF under Award Number DMR 1728858 and NSF-MRSEC Program under Award Number DMR 142007.

Notes

The authors declare no competing financial interest.

DOI: 10.1021/acs.biomac.9b00107
Biomacromolecules 2019, 20, 3340−3351

■ ACKNOWLEDGMENTS

The authors thank Dr. Jeffrey F. Morris and Omer Sedes of the Chemical Engineering department at The City College of New York for their assistance with rheology experiments as well as Dr. Ken Dill from the Laufer Center for Physical and Quantitative Biology at Stony Brook University for helpful insight into the UCST. The authors also thank Andrew Olsen for his assistance in microrheology experiments and Dr. César A. Berríos-Otero for his assistance in data processing. This research used resources of the Center for Functional Nanomaterials, which is a U.S. DOE Office of Science Facility, at the Brookhaven National Laboratory under Contract No. DE-SC0012704 for TEM measurements. SEM and ATR-FTIR experiments were performed at the NYU Chemistry Department Shared Instrument Facility. This work was also supported in part through the NYU IT High Performance Computing resources, services, and staff expertize.

■ REFERENCES

(1) Buwalda, S. J.; Vermonden, T.; Hennink, W. E. Hydrogels for Therapeutic Delivery: Current Developments and Future Directions. *Biomacromolecules* **2017**, *18*, 316−330.
(2) Wichterle, O.; Lím, D. Hydrophilic Gels for Biological Use. *Nature* **1960**, *185*, 117−118.
(3) Sengupta, D.; Heilshorn, S. C. Protein-Engineered Biomaterials: Highly Tunable Tissue Engineering Scaffolds. *Tissue Eng., Part B* **2010**, *16*, 285−293.
(4) De Leon Rodriguez, L. M.; Hemar, Y.; Cornish, J.; Brimble, M. A. Structure-Mechanical Property Correlations of Hydrogel Forming β-Sheet Peptides. *Chem. Soc. Rev.* **2016**, *45*, 4797−4824.
(5) Cohen, C.; Parry, D. A. Alpha-Helical Coiled Coils: More Facts and Better Predictions. *Science* **1994**, *263*, 488−489.
(6) Kopeček, J.; Yang, J. Smart Self-Assembled Hybrid Hydrogel Biomaterials. *Angew. Chem., Int. Ed.* **2012**, *51*, 7396−7417.
(7) Jing, P.; Rudra, J. S.; Herr, A. B.; Collier, J. H. Self-Assembling Peptide-Polymer Hydrogels Designed from the Coiled Coil Region of Fibrin. *Biomacromolecules* **2008**, *9*, 2438−2446.
(8) Rudra, J. S.; Tripathi, P. K.; Hildeman, D. A.; Jung, J. P.; Collier, J. H. Immune Responses to Coiled Coil Supramolecular Biomaterials. *Biomaterials* **2010**, *31*, 8475−8483.
(9) Petka, W. A.; Harden, J. L.; McGrath, K. P.; Wirtz, D.; Tirrell, D. A. Reversible Hydrogels from Self-Assembling Artificial Proteins. *Science* **1998**, *281*, 389−392.
(10) Mi, L.; Fischer, S.; Chung, B.; Sundelacruz, S.; Harden, J. L. Self-Assembling Protein Hydrogels with Modular Integrin Binding Domains. *Biomacromolecules* **2006**, *7*, 38−47.
(11) Kennedy, S. B.; Littrell, K.; Thiyagarajan, P.; Tirrell, D. A.; Russell, T. P. Controlled Structure in Artificial Protein Hydrogels. *Macromolecules* **2005**, *38*, 7470−7475.
(12) Olsen, B. D.; Kornfield, J. A.; Tirrell, D. A. Yielding Behavior in Injectable Hydrogels from Telechelic Proteins. *Macromolecules* **2010**, *43*, 9094−9099.
(13) Olsen, A. J.; Katyal, P.; Haghpanah, J. S.; Kubilius, M. B.; Li, R.; Schnabel, N. L.; O'Neill, S. C.; Wang, Y.; Dai, M.; Singh, N.; Tu, R. S.; Montclare, J. K. Protein Engineered Triblock Polymers Composed of Two Sads: Enhanced Mechanical Properties and Binding Abilities. *Biomacromolecules* **2018**, *19*, 1552−1561.
(14) Wheeldon, I. R.; Barton, S. C.; Banta, S. Bioactive Proteinaceous Hydrogels from Designed Bifunctional Building Blocks. *Biomacromolecules* **2007**, *8*, 2990−2994.
(15) Shen, W.; Lammertink, R. G. H.; Sakata, J. K.; Kornfield, J. A.; Tirrell, D. A. Assembly of an Artificial Protein Hydrogel through Leucine Zipper Aggregation and Disulfide Bond Formation. *Macromolecules* **2005**, *38*, 3909−3916.
(16) Xu, C.; Breedveld, V.; Kopecek, J. Reversible Hydrogels from Self-Assembling Genetically Engineered Protein Block Copolymers. *Biomacromolecules* **2005**, *6*, 1739−1749.
(17) Xu, C.; Kopecek, J. Genetically Engineered Block Copolymers: Influence of the Length and Structure of the Coiled-Coil Blocks on Hydrogel Self-Assembly. *Pharm. Res.* **2008**, *25*, 674−682.
(18) Huang, C.-C.; Ravindran, S.; Yin, Z.; George, A. 3-D Self-Assembling Leucine Zipper Hydrogel with Tunable Properties for Tissue Engineering. *Biomaterials* **2014**, *35*, 5316−5326.
(19) Potekhin, S. A.; Melnik, T. N.; Popov, V.; Lanina, N. F.; Vazina, A. A.; Rigler, P.; Verdini, A. S.; Corradin, G.; Kajava, A. V. De Novo Design of Fibrils Made of Short Alpha-Helical Coiled Coil Peptides. *Chem. Biol.* **2001**, *8*, 1025−1032.
(20) Fletcher, N. L.; Lockett, C. V.; Dexter, A. F. A PH-Responsive Coiled-Coil Peptide Hydrogel. *Soft Matter* **2011**, *7*, 10210.
(21) Banwell, E. F.; Abelardo, E. S.; Adams, D. J.; Birchall, M. A.; Corrigan, A.; Donald, A. M.; Kirkland, M.; Serpell, L. C.; Butler, M. F.; Woolfson, D. N. Rational Design and Application of Responsive Alpha-Helical Peptide Hydrogels. *Nat. Mater.* **2009**, *8*, 596−600.
(22) Mehrban, N.; Zhu, B.; Tamagnini, F.; Young, F. I.; Wasmuth, A.; Hudson, K. L.; Thomson, A. R.; Birchall, M. A.; Randall, A. D.; Song, B.; Woolfson, D. N. Functionalized α-Helical Peptide Hydrogels for Neural Tissue Engineering. *ACS Biomater. Sci. Eng.* **2015**, *1*, 431−439.
(23) Wang, C.; Kopecek, J.; Stewart, R. J. Hybrid Hydrogels Cross-Linked by Genetically Engineered Coiled-Coil Block Proteins. *Biomacromolecules* **2001**, *2*, 912−920.
(24) Yang, J.; Xu, C.; Wang, C.; Kopecek, J. Refolding Hydrogels Self-Assembled from N-(2-Hydroxypropyl)Methacrylamide Graft Copolymers by Antiparallel Coiled-Coil Formation. *Biomacromolecules* **2006**, *7*, 1187−1195.
(25) Yang, J.; Xu, C.; Kopecková, P.; Kopecek, J. Hybrid Hydrogels Self-Assembled from HPMA Copolymers Containing Peptide Grafts. *Macromol. Biosci.* **2006**, *6*, 201−209.
(26) Yang, J.; Wu, K.; Konák, C.; Kopecek, J. Dynamic Light Scattering Study of Self-Assembly of HPMA Hybrid Graft Copolymers. *Biomacromolecules* **2008**, *9*, 510−517.
(27) Wu, K.; Yang, J.; Liu, J.; Kopeček, J. Coiled-Coil Based Drug-Free Macromolecular Therapeutics: In Vivo Efficacy. *J. Controlled Release* **2012**, *157*, 126−131.
(28) Zhang, R.; Yang, J.; Chu, T.-W.; Hartley, J. M.; Kopeček, J. Multimodality Imaging of Coiled-Coil Mediated Self-Assembly in a "Drug-Free" Therapeutic System. *Adv. Healthcare Mater.* **2015**, *4*, 1054−1065.
(29) Chu, T.-W.; Feng, J.; Yang, J.; Kopeček, J. Hybrid Polymeric Hydrogels via Peptide Nucleic Acid (PNA)/DNA Complexation. *J. Controlled Release* **2015**, *220*, 608−616.
(30) Peppas, N. A.; Bures, P.; Leobandung, W.; Ichikawa, H. Hydrogels in Pharmaceutical Formulations. *Eur. J. Pharm. Biopharm.* **2000**, *50*, 27−46.
(31) Wang, H.; Heilshorn, S. C. Adaptable Hydrogel Networks with Reversible Linkages for Tissue Engineering. *Adv. Mater.* **2015**, *27*, 3717−3736.
(32) Banta, S.; Wheeldon, I. R.; Blenner, M. Protein Engineering in the Development of Functional Hydrogels. *Annu. Rev. Biomed. Eng.* **2010**, *12*, 167−186.
(33) Echeverria, C.; Fernandes, S.; Godinho, M.; Borges, J.; Soares, P. Functional Stimuli-Responsive Gels: Hydrogels and Microgels. *Gels* **2018**, *4*, No. 54.
(34) Su, R. S.-C.; Kim, Y.; Liu, J. C. Resilin: Protein-Based Elastomeric Biomaterials. *Acta Biomater.* **2014**, *10*, 1601−1611.
(35) Hume, J.; Sun, J.; Jacquet, R.; Renfrew, P. D.; Martin, J. A.; Bonneau, R.; Gilchrist, M. L.; Montclare, J. K. Engineered Coiled-Coil Protein Microfibers. *Biomacromolecules* **2014**, *15*, 3503−3510.
(36) More, H. T.; Zhang, K. S.; Srivastava, N.; Frezzo, J. A.; Montclare, J. K. Influence of Fluorination on Protein-Engineered Coiled-Coil Fibers. *Biomacromolecules* **2015**, *16*, 1210−1217.
(37) Link, A. J.; Tirrell, D. A. Cell Surface Labeling of *Escherichia coli* via Copper(I)-Catalyzed [3+2] Cycloaddition. *J. Am. Chem. Soc.* **2003**, *125*, 11164−11165.
(38) Tanrikulu, I. C.; Schmitt, E.; Mechulam, Y.; Goddard, W. A.; Tirrell, D. A. Discovery of *Escherichia coli* Methionyl-TRNA

DOI: 10.1021/acs.biomac.9b00107
Biomacromolecules 2019, 20, 3340−3351

Synthetase Mutants for Efficient Labeling of Proteins with Azidonorleucine in Vivo. *Proc. Natl. Acad. Sci. U.S.A.* **2009**, *106*, 15285−15290.
(39) Sankaram, M. B.; Marsh, D.; Thompson, T. E. Determination of Fluid and Gel Domain Sizes in Two-Component, Two-Phase Lipid Bilayers. An Electron Spin Resonance Spin Label Study. *Biophys. J.* **1992**, *63*, 340−349.
(40) Zhang, S.; Zhang, L.; Bouzid, M.; Rocklin, Z.; Del Gado, E.; Mao, X. Correlated Rigidity Percolation and Colloidal Gels 2018, arXiv:1807.08858. arXiv.org e-Print archive. http://arxiv.org/abs/1807.08858.
(41) Niskanen, J.; Tenhu, H. How to Manipulate the Upper Critical Solution Temperature (UCST)? *Polym. Chem.* **2017**, *8*, 220−232.
(42) O'Neill, S. C.; Bhuiyan, Z. H.; Tu, R. S. Evolution of Mechanics in α-Helical Peptide Conjugated Linear- and Star-Block PEG. *Soft Matter* **2017**, *13*, 7521−7528.
(43) Larsen, T. H.; Furst, E. M. Microrheology of the Liquid-Solid Transition during Gelation. *Phys. Rev. Lett.* **2008**, *100*, No. 146001.
(44) Dufresne, E. R.; Squires, T. M.; Brenner, M. P.; Grier, D. G. Hydrodynamic Coupling of Two Brownian Spheres to a Planar Surface. *Phys. Rev. Lett.* **2000**, *85*, 3317−3320.
(45) Pelletier, V.; Gal, N.; Fournier, P.; Kilfoil, M. L. Microrheology of Microtubule Solutions and Actin-Microtubule Composite Networks. *Phys. Rev. Lett.* **2009**, *102*, No. 188303.
(46) Sathaye, S.; Mbi, A.; Sonmez, C.; Chen, Y.; Blair, D. L.; Schneider, J. P.; Pochan, D. J. Rheology of Peptide- and Protein-Based Physical Hydrogels: Are Everyday Measurements Just Scratching the Surface? *Wiley Interdiscip. Rev.: Nanomed. Nanobiotechnol.* **2015**, *7*, 34−68.
(47) Schultz, K. M.; Anseth, K. S. Monitoring Degradation of Matrix Metalloproteinases-Cleavable PEG Hydrogels via Multiple Particle Tracking Microrheology. *Soft Matter* **2013**, *9*, 1570−1579.
(48) Martin, J. E.; Adolf, D.; Wilcoxon, J. P. Viscoelasticity of Near-Critical Gels. *Phys. Rev. Lett.* **1988**, *61*, 2620−2623.
(49) Martin, J. E.; Adolf, D. Diffusion in Branched Polymer Melts. *Macromolecules* **1989**, *22*, 4309−4311.
(50) Martin, J. E.; Adolf, D.; Wilcoxon, J. P. Viscoelasticity near the Sol-Gel Transition. *Phys. Rev. A* **1989**, *39*, 1325−1332.
(51) Adolf, D.; Martin, J. E. Time-Cure Superposition during Crosslinking. *Macromolecules* **1990**, *23*, 3700−3704.
(52) Kothiwale, S.; Mendenhall, J. L.; Meiler, J. BCL::Conf: Small Molecule Conformational Sampling Using a Knowledge Based Rotamer Library. *J. Cheminf.* **2015**, *7*, No. 47.
(53) DeLuca, S.; Khar, K.; Meiler, J. Fully Flexible Docking of Medium Sized Ligand Libraries with RosettaLigand. *PLoS One* **2015**, *10*, No. e0132508.
(54) Yuan, S.; Lei, F.; Liu, Z.; Tong, Q.; Si, T.; Xu, R. X. Coaxial Electrospray of Curcumin-Loaded Microparticles for Sustained Drug Release. *PLoS One* **2015**, *10*, No. e0132609.
(55) Brazel, C. S.; Peppas, N. A. Modeling of Drug Release from Swellable Polymers. *Eur. J. Pharm. Biopharm.* **2000**, *49*, 47−58.
(56) Lapidus, H.; Lordi, N. G. Some Factors Affecting the Release of a Water-Soluble Drug from a Compressed Hydrophilic Matrix. *J. Pharm. Sci.* **1966**, *55*, 840−843.
(57) Higuchi, T. Mechanism of Sustained-Action Medication. Theoretical Analysis of Rate of Release of Solid Drugs Dispersed in Solid Matrices. *J. Pharm. Sci.* **1963**, *52*, 1145−1149.
(58) Hixson, A. W.; Crowell, J. H. Dependence of Reaction Velocity upon Surface and Agitation. *Ind. Eng. Chem.* **1931**, *23*, 923−931.
(59) Korsmeyer, R. W.; Gurny, R.; Doelker, E.; Buri, P.; Peppas, N. A. Mechanisms of Solute Release from Porous Hydrophilic Polymers. *Int. J. Pharm.* **1983**, *15*, 25−35.
(60) Bugatti, V.; Vertuccio, L.; Viscusi, G.; Gorrasi, G. Antimicrobial Membranes of Bio-Based PA 11 and HNTs Filled with Lysozyme Obtained by an Electrospinning Process. *Nanomaterials* **2018**, *8*, No. 139.
(61) Mashak, A.; Mobedi, H.; Mahdavi, H. A Comparative Study of Progesterone and Lidocaine Hydrochloride Release from Poly(L-Lactide) Films. *Pharm. Sci.* **2015**, *21*, 77−85.
(62) Ritger, P. L.; Peppas, N. A. A Simple Equation for Description of Solute Release II. Fickian and Anomalous Release from Swellable Devices. *J. Controlled Release* **1987**, *5*, 37−42.
(63) Hu, X.; Kaplan, D.; Cebe, P. Determining Beta-Sheet Crystallinity in Fibrous Proteins by Thermal Analysis and Infrared Spectroscopy. *Macromolecules* **2006**, *39*, 6161−6170.
(64) Haghpanah, J. S.; Yuvienco, C.; Civay, D. E.; Barra, H.; Baker, P. J.; Khapli, S.; Voloshchuk, N.; Gunasekar, S. K.; Muthukumar, M.; Montclare, J. K. Artificial Protein Block Copolymers Blocks Comprising Two Distinct Self-Assembling Domains. *ChemBioChem* **2009**, *10*, 2733−2735.
(65) Dai, M.; Haghpanah, J.; Singh, N.; Roth, E. W.; Liang, A.; Tu, R. S.; Montclare, J. K. Artificial Protein Block Polymer Libraries Bearing Two SADs: Effects of Elastin Domain Repeats. *Biomacromolecules* **2011**, *12*, 4240−4246.
(66) Yuvienco, C.; More, H. T.; Haghpanah, J. S.; Tu, R. S.; Montclare, J. K. Modulating Supramolecular Assemblies and Mechanical Properties of Engineered Protein Materials by Fluorinated Amino Acids. *Biomacromolecules* **2012**, *13*, 2273−2278.
(67) Hill, L. K.; Frezzo, J. A.; Katyal, P.; Hoang, D. M.; Ben Youss Gironda, Z.; Xu, C.; Xie, X.; Delgado-Fukushima, E.; Wadghiri, Y. Z.; Montclare, J. K. Protein-Engineered Nanoscale Micelles for Dynamic 19F Magnetic Resonance and Therapeutic Drug Delivery. *ACS Nano* **2019**, *13*, 2969−2985.
(68) Savitzky, A.; Golay, M. J. E. Smoothing and Differentiation of Data by Simplified Least Squares Procedures. *Anal. Chem.* **1964**, *36*, 1627−1639.
(69) Gunasekar, S. K.; Asnani, M.; Limbad, C.; Haghpanah, J. S.; Hom, W.; Barra, H.; Nanda, S.; Lu, M.; Montclare, J. K. N-Terminal Aliphatic Residues Dictate the Structure, Stability, Assembly, and Small Molecule Binding of the Coiled-Coil Region of Cartilage Oligomeric Matrix Protein. *Biochemistry* **2009**, *48*, 8559−8567.
(70) Kwok, S. C.; Hodges, R. S. Stabilizing and Destabilizing Clusters in the Hydrophobic Core of Long Two-Stranded Alpha-Helical Coiled-Coils. *J. Biol. Chem.* **2004**, *279*, 21576−21588.
(71) Schneider, C. A.; Rasband, W. S.; Eliceiri, K. W. NIH Image to ImageJ: 25 Years of Image Analysis. *Nat. Methods* **2012**, *9*, 671−675.
(72) Wheeldon, I. R.; Campbell, E.; Banta, S. A Chimeric Fusion Protein Engineered with Disparate Functionalities-Enzymatic Activity and Self-Assembly. *J. Mol. Biol.* **2009**, *392*, 129−142.
(73) Hume, J.; Chen, R.; Jacquet, R.; Yang, M.; Montclare, J. K. Tunable Conformation-Dependent Engineered Protein·Gold Nanoparticle Nanocomposites. *Biomacromolecules* **2015**, *16*, 1706−1713.
(74) Baker, N. A.; Sept, D.; Joseph, S.; Holst, M. J.; McCammon, J. A. Electrostatics of Nanosystems: Application to Microtubules and the Ribosome. *Proc. Natl. Acad. Sci. U.S.A.* **2001**, *98*, 10037−10041.
(75) DeLano, W. L. The PyMOL Molecular Graphics System, 2002. http://www.pymol.org.
(76) Chassenieux, C.; Tsitsilianis, C. Recent Trends in PH/Thermo-Responsive Self-Assembling Hydrogels: From Polyions to Peptide-Based Polymeric Gelators. *Soft Matter* **2016**, *12*, 1344−1359.
(77) Marek, S. R.; Gran, M. L.; Peppas, N. A.; Caldorera-Moore, M. Intelligent, Responsive and Theranostic Hydrogel Systems for Controlled Delivery of Therapeutics. In *Chemoresponsive Materials*; Schneider, H.-J., Ed.; RSC Smart Materials; Royal Society of Chemistry: Cambridge, 2015; Chapter 2, pp 10−43.
(78) Klouda, L.; Mikos, A. G. Thermoresponsive Hydrogels in Biomedical Applications. *Eur. J. Pharm. Biopharm.* **2008**, *68*, 34−45.
(79) Weng, L.; Chen, X.; Chen, W. Rheological Characterization of in Situ Crosslinkable Hydrogels Formulated from Oxidized Dextran and N-Carboxyethyl Chitosan. *Biomacromolecules* **2007**, *8*, 1109−1115.
(80) Tatulian, S. A. Structural Characterization of Membrane Proteins and Peptides by FTIR and ATR-FTIR Spectroscopy. *Methods Mol. Biol.* **2013**, *974*, 177−218.
(81) Gunasekar, S. K.; Anjia, L.; Matsui, H.; Montclare, J. K. Effects of Divalent Metals on Nanoscopic Fiber Formation and Small Molecule Recognition of Helical Proteins. *Adv. Funct. Mater.* **2012**, *22*, 2154−2159.

DOI: 10.1021/acs.biomac.9b00107
Biomacromolecules 2019, 20, 3340−3351

(82) Wang, C.; Stewart, R. J.; Kopecek, J. Hybrid Hydrogels Assembled from Synthetic Polymers and Coiled-Coil Protein Domains. *Nature* **1999**, *397*, 417−420.
(83) Bae, Y. C.; Shim, J. J.; Soane, D. S.; Prausnitz, J. M. Representation of Vapor−liquid and Liquid−liquid Equilibria for Binary Systems Containing Polymers: Applicability of an Extended Flory−huggins Equation. *J. Appl. Polym. Sci.* **1993**, *47*, 1193−1206.
(84) Natarajan, J. V.; Nugraha, C.; Ng, X. W.; Venkatraman, S. Sustained-Release from Nanocarriers: A Review. *J. Controlled Release* **2014**, *193*, 122−138.

DOI: 10.1021/acs.biomac.9b00107
Biomacromolecules 2019, 20, 3340−3351